# Atomistic mechanism of interfacial reaction and asymmetric growth kinetics in an immiscible Cu-Ru system at equilibrium

Xiang He, Su-Hui Liang, Jia-Hao Li, and Bai-Xin Liu*
*Advanced Materials Laboratory, Department of Materials Science and Engineering, Tsinghua University, Beijing 100084, China*
(Received 11 July 2006; revised manuscript received 18 October 2006; published 26 January 2007)

An *n*-body potential is first constructed for the immiscible Cu-Ru system at equilibrium with the aid of *ab initio* calculations for obtaining some physical properties necessary to fit the Cu-Ru cross-potential. Molecular dynamics simulations are then performed to pursue atomistic modeling of interfacial reaction between the Cu-Ru metal layers. Using the solid solution model, simulations reveal that the Cu-based and the Ru-based solid solutions collapse at their respective critical solid solubilities, i.e., 10 at. % of Ru and 20 at. % of Cu, thus determining an intrinsic glass-forming range of the system to be within 10–80 at. % Ru, which matches well with the observations in ion-beam mixing experiments. Using the Cu-Ru sandwich model, simulations clarify that the interfacial free energy is the major driving force for interfacial reaction, resulting in spontaneous solid-state amorphization and that when the interfacial free energy is completely consumed, the reaction terminates, thus determining a maximum amorphous interlayer to be 2.91 nm, which is in good agreement with that predicted from a recently proposed thermodynamic and kinetic model. Kinetically, simulations further reveal that the growth of the amorphous interlayer features an asymmetric behavior, i.e., the growth advances faster toward the Cu lattice than toward the Ru side, because the critical solid solubility of Ru in Cu (10 at. %) is smaller than that of Cu in Ru (20 at. %).

DOI: 10.1103/PhysRevB.75.045431 PACS number(s): 68.55.−a, 05.70.Np, 31.15.Qg

## I. INTRODUCTION

Copper has attracted much attention during past decades in the integrated circuits industry, as Cu has been used as an interconnection metal to replace aluminum in microelectronic circuits due to its favorable electrical conductivity and superior resistance to electromigration.[1] To prevent catastrophic contamination caused by Cu diffusing through interlayer dielectrics into silicon, diffusion barriers, such as tantalum and tantalum nitride (Ta/TaN), are currently used to protect the Cu interconnects.[2,3] As the trend of miniaturization continues in microelectronic fabrication, the current Ta/TaN diffusion barrier for Cu interconnects will encounter scaling difficulties at the 45 nm node. To maintain a low effective interconnect resistivity, an ultrathin diffusion barrier (about 5 nm) is needed to scale the next-generation integrated circuit technology for the 45 nm node.[4]

Ruthenium is an air-stable transition metal with a high melting point (2583 K) and is nearly twice as thermally and electrically conductive (7.6 $\mu\Omega$ cm) as Ta. More importantly, the Cu-Ru system is an essentially immiscible one characterized with a positive heat of formation ($\Delta H_f$) of +10.44 kJ/mol calculated by Miedema's model.[5] Recently, there has been an increasing interest to utilize Ru as a Cu-plateable diffusion barrier.[6–8] Some researchers showed that the inherently favorable interfacial bonding manifested in the strong adhesion between the electroplated Cu and Ru substrate, even when annealing to over 870 K.[9] Obviously, the advent of solid-state amorphization would definitely degrade the performances of the electronic devices. Under such circumstances, theoretical modeling concerning the interfacial reaction between Cu and Ru is therefore of importance. On the other hand, the formation of any Cu-Ru metastable phase could bring about some effects to degrade the performance of Ru as a diffusion barrier, as well as of Cu as an interconnection in the electronic devices. It is therefore of both practical and theoretical importance to have a thorough investigation of the Cu-Ru system concerning the metastable phase formation, the interfacial stability, and the associated underlying physics for a deep understanding.

In synthesizing new nonequilibrium alloys, ion beam mixing (IBM) of multiple metal layers was introduced in early 1980s, and due to its very powerful capability, IBM has so far produced a variety of nonequilibrium alloys in numerous binary metal systems. Recently, IBM has been focused on studying the binary metal systems characterized by large positive $\Delta H_f$, and the systems are essentially immiscible at equilibrium. To increase the interfacial free energy stored in the multilayered samples, the individual layer thickness was intentionally designed to be a couple of nanometers, differing considerably from the typical thickness of 5–8 nm in the previously conducted IBM. Accordingly, the interfacial free energy played an important role in elevating the initial multilayered films to an energetic level higher than those of the possible metastable states existing in the system of interest.[10]

In the present study, thermodynamic calculation is conducted, based on Miedema's model, to give macroscopic insight concerning the formation of the metastable phases by comparing the relative energetic levels of the competing phases in question. In atomistic modeling, with an aid of *ab initio* calculations for acquiring some physical data, a tight-binding potential of the Cu-Ru system is constructed and applied in molecular dynamic (MD) simulations to determine the glass-formation ability/range (GFA/GFR) of the system and to reveal the atomistic mechanism of interface stability and SSA of the Cu-Ru system. A brief discussion follows to compare the results of the theoretical modeling with the experimental observations.

 

## II. CALCULATION METHODS AND EXPERIMENTAL PROCEDURE

### A. Thermodynamic calculation

Generally, the Gibbs free energy of an alloy phase can be calculated by $\Delta G=\Delta H-T\cdot\Delta S$, where $\Delta H$ and $\Delta S$ are the enthalpy and entropy terms, respectively. As a first approximation, the entropy term for a concentrated solid solution (CSS) and amorphous phase is simply taken as that of an ideal solution, i.e., $\Delta S=-R[c_A\ln c_A+c_B\ln c_B]$, where R is the gas constant and $c_A$ and $c_B$ are the atomic concentrations of metals A and B, respectively.

According to Miedema's model and Alonso's method,[5,11–13] the enthalpy change $\Delta H$ is the sum of three terms, namely, $\Delta H=\Delta H^c+\Delta H^e+\Delta H^s$, corresponding to the chemical, elastic, and structural contributions, respectively. The chemical term $\Delta H^c$ is closely related to the electron redistribution generated at the boundary for the Wigner–Seitz unit cell when alloying, and can be calculated by

$$\Delta H^c = c_A c_B[c_B \Delta \bar{H}^{inter}_{AinB} + c_A \Delta \bar{H}^{inter}_{BinA}], \tag{1}$$

where $\Delta \bar{H}^{inter}_{AinB}$ and $\Delta \bar{H}^{inter}_{BinA}$ are the solution enthalpies of A solved in B and that of B solved in A, respectively, and all these values have been compiled by de Boer *et al.*[5] and Bakker.[11]

The elastic term $\Delta H^e$ for a CSS is caused by the atomic size mismatch of the two constituent metals and can be expressed by taking the weighted average of the mismatch energies[5,11]

$$\Delta H^e = c_A c_B[c_B \Delta \bar{H}^{elastic}_{AinB} + c_A \Delta \bar{H}^{elastic}_{BinA}] \tag{2}$$

where $\Delta \bar{H}^{elastic}_{AinB}$ and $\Delta \bar{H}^{elastic}_{BinA}$ are the partial elastic mismatch energies for A solved in B and B solved in A, respectively, and all these values can be found in some published books and/or comprehensive papers.[5,11]

The structure term $\Delta H^s$ is deduced from the lattice stability $E(Z)$ of the bcc, fcc, and hcp structures as a function of the number of valence electrons $Z$ of the metal,[5,11]

$$\Delta H^s = E(Z) - c_A E(Z_B) - c_B E(Z_A), \tag{3}$$

where $E(Z)$, $E(Z_A)$, and $E(Z_B)$ are the lattice stability of the CSS and pure metals A and B, and $Z$, $Z_A$, and $Z_B$ are the mean numbers of valence electrons of the CSS and the numbers of valence electrons of pure metals A and B, respectively.[5,11]

Comparing with the CSS, the structural and elastic terms for the formation enthalpy of an amorphous alloy are absent or significantly reduced, i.e., $\Delta H^e \approx 0$ and $\Delta H^s \approx 0$.[5,11] There is, however, apart from the chemical term, another term contributing to the formation enthalpy of the amorphous alloy that reflects the relative disordering and therefore the formation enthalpy of the amorphous alloy can be expressed by[5,11]

$$\Delta H^{amorphous} = \Delta H^c + \Delta H^{topological}, \tag{4}$$

where the topological enthalpy $\Delta H^{topological}$ accounts for the difference between the crystalline and amorphous states, which can be calculated by [5,11]

$$\Delta H^{topological} = 3.5(c_A T_{m,A} + c_B T_{m,B}), \tag{5}$$

where $T_{m,A}$ and $T_{m,B}$ are the melting temperatures of the metals A and B, respectively. Meanwhile, the chemical term of the amorphous alloy $\Delta H^c$ can be assumed to be equal to that of the CSS.

For a system with metals A and B, the Gibbs free energy of the initial state of the A-B multilayered samples should be calculated by adding the interfacial free energy to the ground state (i.e., the zero line) representing a mechanical mixture of A and B in the bulk form. According to Zhang *et al.*,[5,14–16] the excess interfacial free energy of the multilayered samples can be calculated by $\Delta G_{mul}=\alpha_A S_{fA}\gamma^{SS}_{BA}+\alpha_B S_{fB}\gamma^{SS}_{AB}$, where $S_{fA}$ and $S_{fB}$ are the surface areas occupied by one mole of atoms A and B, respectively; $\alpha_A$ and $\alpha_B$ are the fraction of the interfacial atoms A and B versus the total number of atoms in the A-B multilayered samples; and $\gamma^{SS}_{AB}$ (or $\gamma^{SS}_{BA}$) are the interfacial free energy of one mole of atoms A (or B) solved in B (or A). These terms can easily be calculated following the well-documented literature.[5,14–16]

### B. *Ab initio* calculation

Since we are dealing with the equilibrium immiscible Cu-Ru system, for which there are very few available experimental data related to the Cu-Ru compounds, it is a challenging task to fit the Cu-Ru cross potential. In this respect, the first-principle calculation based on quantum mechanics is known to be a reliable way to acquire some physical properties of some possible Cu-Ru compounds in question. In the calculations, we employed the Vienna *ab initio* simulation package VASP,[17–19] of which the PAW pseudopotentials have been constructed by considering the all-electrons effect. The exchange and correlation effects were described by the functional proposed by Perdew and Zunger,[20] employing the generalized gradient corrections.[21] Brillouin-zone integrations were performed using an $11\times11\times11$ Monkhorst–Pack[22] grid, leading to 56 irreducible $k$ points. A plane-wave cutoff energy was set to be 341.6 eV. Besides, for all spin-polarized calculations, the Vosko–Wilk–Nusair interpolations were used for the correlation part of the exchange correlation functional.[23]

### C. Construction of *n*-body Cu-Ru potential

The tight-binding potential, namely, the second-moment approximation of the tight-binding scheme (TB-SMA), is adopted to construct the $n$-body Cu-Ru potential, as the scheme has successfully been employed in a large number of fcc and/or hcp transition metals.[24–26] In the TB-SMA scheme, the repulsive portion is a Born–Mayer pairwise interaction and the attractive portion is a second-moment approximation of the tight-binding band energy. The cohesive and repulsive items of the total energy are exponential functions of the atomic distance as written below:

$$E_{total} = \sum_i \left\{ \sum_{j \neq i} A_{\alpha\beta} \exp\left[ -p_{\alpha\beta}\left( \frac{r_{ij}}{r_{\alpha\beta}} - 1 \right) \right] - \sqrt{\sum_{j \neq i} \xi_{\alpha\beta}^2 \exp\left[ -2q_{\alpha\beta}\left( \frac{r_{ij}}{r_{\alpha\beta}} - 1 \right) \right]} \right\}, \quad (6)$$

where $\alpha$ and $\beta$ indicate the atomic species, $r_{ij}$ is the distance between atoms $i$ and $j$, and is calculated up to a distance $r_{cutoff}$, whereas $r_{\alpha\beta}$ is taken to be the nearest distance between atoms $\alpha$ and $\beta$ in the crystal structure. $A_{\alpha\beta}$, $p_{\alpha\beta}$, $\xi_{\alpha\beta}$, and $q_{\alpha\beta}$ are adjustable potential parameters, which are generally determined by fitting to their respective physical properties. In the present study, these parameters are determined as follows: (i) For $\alpha=\beta$, the fitting procedures are performed on the cohesive energies, lattice constants, and elastic moduli at 0 K for the pure Cu and Ru metals. The parameters $r_{\alpha\alpha}$ and $r_{\beta\beta}$ are taken to be the nearest-neighbor distance, i.e., $r_0$, of the pure Cu and Ru metals, respectively. (ii) For $\alpha \neq \beta$, the corresponding parameters are fitted to the *ab initio* acquired lattice constants, cohesive energies elastic, and bulk moduli of the metastable $L1_2$ $Cu_3Ru$ and $CuRu_3$ compounds.

### D. Scheme of molecular dynamics simulation and simulations models

In the present study, MD simulation is carried out with Parrinello–Rahman constant pressure scheme and the equations of motion are solved using a fourth-order predictor-corrector algorithm of Gear with a time step $t=5\times10^{-15}$ s.[27,28] For a series of solid solutions with various compositions, the MD simulation is performed at 300 K and at zero pressure for 50 000–150 000 MD time steps to reach a relatively equilibrium (metastable) state, at which all the related dynamic variables show no secular variation. The process of structural change in the solid solution models is monitored by the pair-correlation functions $g(r)$.[29] Meanwhile, another indicator of structural change, namely, the planar structure factor $S(\mathbf{k},\mathbf{z})$, is also calculated to provide evidence of the structural change. Moreover, density profiles $\rho_\alpha(z)$ of each species along the z direction are also used to monitor the structural changes of interest.[30]

We use two types of simulation models in the present study, i.e., the solid solution model and the sandwich model.

In the first type, the simulation models are set to be the fcc and hcp solid solutions, respectively. The fcc solid solution models consist of $8\times8\times8\times4=2048$ atoms, and the hcp solid solution models consist of $10\times6\times6\times4=1440$ atoms, respectively. In both fcc and hcp models, the [100] and [001] crystalline directions are parallel to the $x$ and $z$ axes, respectively, and the crystalline directions along the $y$ axis are [010] for fcc Cu and [120] for hcp Ru, respectively. The periodic boundary conditions are adopted in all three directions. In setting the solid solution models, the solute atoms are added by random substitution to a desired number of Ru (Cu) atoms into the Cu fcc (Ru hcp), obtaining the initial state of fcc Cu-rich (hcp Ru-rich) solid solution model.

In the second type to represent the real multilayered films used in experiments, the sandwich models are constructed by stacking, along the $z$ axis, 10 fcc Cu (100) planes, 12 hcp Ru $(01\bar{1}0)$, and 10 fcc Cu (100) planes, which all parallel to the $x$-$y$ plane. Two interfaces thus locate at no. 10-11 and no. 22-23 atomic planes. The crystalline direction [100] of fcc Cu and [2 -1 -1 0] of hcp Ru with the units distances of 3.615 and 2.704 Å, respectively, are arranged to be parallel to the $x$ axis, leading to a size difference ratio of 1.337. Meanwhile, the crystalline direction [010] of fcc Cu and [0001] of hcp Ru with units distances of 3.615 and 4.282 Å, respectively, are arranged to parallel to the $y$ axis, leading to a size difference ratio of 0.844. Considering the simulation to be under a manageable scale, the numbers of Cu and Ru atoms in the $x$-$y$ plane are selected to be $10\times10\times2=200$ atoms and $13\times8\times3=312$ atoms, respectively, resulting in a lattice difference ratio of 1.337 in $x$ axis and 0.844 in $y$ axis, respectively, which are reasonably close to the above-mentioned real situation. The periodic conditions along the $x$ and $y$ directions are set by the larger lattice dimensions of the two lattices, and it has been proved that the influence of the resultant misfit could be neglected.[31,32] The periodic condition is also employed for the $z$ direction and two Cu lattices in the model are therefore adhered together to form a united lattice. The numbers of Cu and Ru atoms in the sandwich model are 4000 and 1248, respectively. In practice, the interface between the two metals is frequently a thin transient layer, which has been proven in experiments to be a disordered state.[33] To have the sandwich model to include such a disordered layer, an equal number of Cu and Ru atoms are artificially exchanged in the interface. After exchanging the Cu and Ru atoms, the sandwich model is annealed at 300 K for $5\times10^6$ MD steps to reach a relatively stable state, at which all the related dynamic variables show no secular variation.

### E. Ion beam mixing

In the present IBM experiment, three sets of Cu-Ru multilayered samples with overall compositions of $Cu_{25}Ru_{75}$, $Cu_{50}Ru_{50}$, $Cu_{75}Ru_{25}$, respectively, are designed, and 200 keV xenon ions are employed as the irradiating ions. According to the TRIM program,[34] the total thickness of the Cu-Ru multilayered films should be designed to be around 45 nm to match the range of the irradiating ions. The $Cu_{25}Ru_{75}$, $Cu_{50}Ru_{50}$, and $Cu_{75}Ru_{25}$ multilayered films consist of 9, 18 (and 12), and 13 layers [i.e., 8, 17 (and 11), and 12 interfaces], respectively, and the thickness of the individual metal layer is therefore in a range of 3–5 nm. The desired compositions of the films are obtained through adjusting the relative thicknesses of the individual Cu and Ru layers. Concerning the details of the calculation of the interfacial free energy and design of the multilayered films, the readers are referred to some previous publications from the authors' group.[35] The intrinsic energy difference of various states, i.e., between the initial Cu-Ru multilayered films and various metastable Cu -Ru phases, is the major thermodynamic driving force for the related structural phase transformation and ion irradiation is to trigger the intermixing between the Cu and Ru layers, resulting in forming the respective metastable Cu-Ru phases. The Cu-Ru multilayered samples are prepared by depositing alternatively pure Cu (99.9%) and Ru (99.9%) at a rate of 0.5 Å/s onto NaCl single crystals as substrates in an e-gun

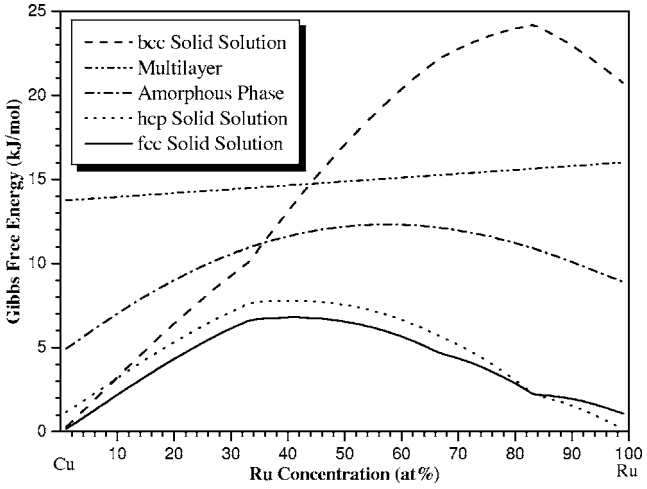


FIG. 1. The calculated Gibbs free energy diagram of the Cu -Ru system based on Miedema's theory and Alonso's method at the temperature of $T=300$ K.

evaporation system with a vacuum level of $10^{-6}$ Pa. The as-deposited Cu-Ru samples are then irradiated by xenon ions in an implanter with a vacuum level better than $5\times10^{-4}$ Pa, and the irradiation dose is in a range from $4\times10^{14}$ to $5\times10^{15}$ $Xe^+/cm^2$. During xenon ion irradiation, the sample holder is cooled by liquid nitrogen (77 K) and the xenon ion current density is confined to be about 2 $\mu A/cm^2$ to minimize an otherwise heating effect. For structural characterization, all the Cu-Ru multilayered samples are removed from the substrates by deionized water and put onto the Cu grids for investigation by room temperature transmission electron microscopy (TEM) bright field examination and selected area diffraction (SAD) analysis to identify the structures in the films. Energy-dispersive spectroscopy (EDS) is also employed to determine the real compositions of the as-deposited films and the resultant alloy phases in the films. In the EDS analysis, the beam spot is about 0.3 $\mu$m, which could be considered the resolution of the measurement, and the measuring error in alloy composition is about 5%.

## III. RESULTS AND DISCUSSION

### A. Calculation of the Gibbs free energy diagram

We first construct a Gibbs free energy diagram of the Cu-Ru system at the temperature of 300 K by calculating the free energy curves of all the alloy phases in question by using the Miedema's model[14] and Alonso's method.[13] Figure 1 shows the calculated Gibbs free energy diagram, in which the energetic state of the Cu-Ru multilayered films containing 18 layers is also included to show the energetic sequence of the initial energetic state of the Cu-Ru multilayered films with the various possible metastable states/phases. From the diagram, one sees that the free energy curve of the amorphous phase is convex like in other systems with large positive $\Delta H_f$. Besides, the initial energetic states of the multilayered films are higher than those of the corresponding solid solution and the amorphous phases over a broad composition range, which are therefore thermodynamically favored to be

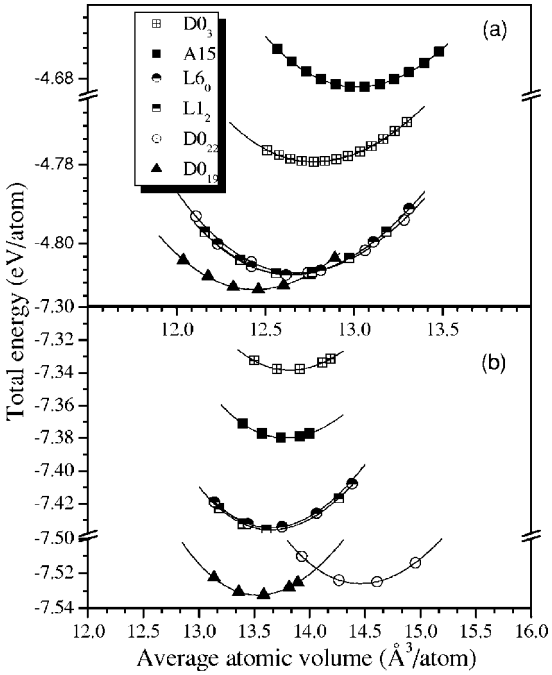


FIG. 2. Correlations of the total energies against the atomic volume of the $Cu_3Ru$ (a) and $CuRu_3$ (b) alloys of some simple structures obtained by *ab initio* calculations.

formed. Moreover, within a composition range of 1–83 at. % of Ru, metastable fcc phase has the lowest free energy than other metastable states, which indicates metastable fcc phase is the most possible to be formed after iron irradiation. Interestingly, by IBM experiments, X. He *et al.* obtained fcc metastable phases in the $Cu_{50}Ru_{50}$ and $Cu_{25}Ru_{75}$ multilayered films, which remained in the fcc structure with increasing the irradiation dose.[36] It can be easily seen that the thermodynamic calculation and experimental results are quite compatible with each other.

### B. *Ab initio* assisted deriving n-body Cu-Ru potential

We then present the results of *ab initio* calculations in acquiring the physical properties of a few possible Cu-Ru compounds. Figure 2(a) shows correlation of total energies against the lattice constant of $CuRu_3$ alloy obtained by *ab initio* calculations within the GGA. From Fig. 2(a), one sees that the A15 structure has the highest positive heat of formation, the $D0_3$ structure is in the second position, the $D0_{19}$, $D0_{22}$, L60, and $L1_2$ structures are almost in a same low energy level, and the $D0_{19}$ structure has the lowest heat of formation among the six studied structures. Interestingly, the relatively stable $L1_2$ structure predicted by above *ab initio* calculations has ever been observed in experiments, i.e., a metastable $Cu_{25}Ru_{75}$ alloy of fcc structure was obtained in thin films upon irradiation and its lattice constants were determined by diffraction analysis to be $a=3.65$ Å,[36] which was compatible with the calculated value of a=3.79 Å. The agreement between the *ab initio* calculation and experimental results, in this respect, could therefore be considered excellent. For the $Cu_{75}Ru_{25}$ alloy, similar results are obtained [Fig. 2(b)], and comparing the results, a metastable$Cu_{75}Ru_{25}$

TABLE I. Comparison of the physical properties of fcc Cu, hcp Ru, $L1_2$ $Cu_3Ru$, and $L1_2$ $CuRu_3$ obtained from *ab initio* calculation, fitted or reproduced from *n*-body potentials and the experimental observation (Refs. 37–39). Lattice constants $a$ and $c$ are expressed in nanometers. Elastic moduli $C_{ij}$ are expressed in Mbar. Cohesive energies $E_c$, and formation $E^f$ energies are expressed in electron volts.

| | | $a$ | $c$ | $E_f$ | $E_c$ | $C_{11}$ | $C_{12}$ | $C_{13}$ | $C_{33}$ | $C_{44}$ |
|---|---|---|---|---|---|---|---|---|---|---|
| fcc Cu | Experimental | 0.361 | | | 3.49 | 1.683 | 1.221 | | | 0.757 |
| | Reproduced | 0.361 | | | 3.58 | 1.690 | 1.218 | | | 0.756 |
| hcp Ru | Experimental | 0.270 | 0.428 | | 6.74 | 5.626 | 1.878 | 1.682 | 6.242 | 1.806 |
| | Reproduced | 0.270 | 0.427 | | 6.70 | 4.647 | 1.736 | 1.974 | 6.725 | 1.559 |
| $L1_2$ $Cu_3Ru$ | CASTEP | 0.368 | | 0.038 | | 1.949 | 1.609 | | | 0.846 |
| | Reproduced | 0.378 | | 0.038 | | 1.876 | 1.701 | | | 0.914 |
| $L1_2$ $CuRu_3$ | CASTEP | 0.370 | | 0.096 | | 3.331 | 2.018 | | | 0.836 |
| | Reproduced | 0.380 | | 0.096 | | 3.350 | 2.160 | | | 0.816 |

alloy of fcc structure was obtained in thin films upon irradiation and its lattice constants were determined by diffraction analysis to be $a=3.60$ Å, which was also compatible with the calculated value of $a=3.70$ Å.

Table I lists the calculated physical properties, such as the lattice constants, the formation energies, as well as the elastic moduli, of the $L1_2$ $Cu_{75}Ru_{25}$ and $L1_2$ $Cu_{25}Ru_{75}$ compounds, together with the experimental properties of fcc Cu and hcp Ru. One notices that the formation of the $L1_2$ $Cu_{75}Ru_{25}$ and $L1_2$ $Cu_{25}Ru_{75}$ compounds are both positive, indicating they are both unstable in an equilibrium state, which is in good agreement with the fact the Cu-Ru system is characterized by a positive $\Delta H_f$ of +10.44 kJ/mol atom. Using the data in the table and the procedure described above, the TB-SMA potential can be derived for the Cu-Ru system. The TB-SMA potential parameters for the Cu-Ru system are listed in Table II. In order to test its relevance, some physical properties of the Cu-Ru system are reproduced using the fitted potential. For convenience of comparison, the reproduced results are also listed in Table I.[37–39] From Table I, one can see obviously that the physical properties fitted or reproduced from the derived *n*-body potential agree with the *ab initio* calculations and/or the experimental results.

### C. Crystal-to-amorphous transition in the Cu-Ru system

#### *1. Glass forming range*

We now present the simulation results for the hcp Ru-based solid solution models first. Figure 3 displays the projections of atomic positions for the $Cu_5Ru_{95}$, $Cu_{20}Ru_{80}$, and $Cu_{50}Ru_{50}$ hcp solid solutions upon annealing at 300 K for 120 000 MD time steps, respectively. From the figure, one sees vividly that for the solid solution with 5 at. % of Cu, the hcp structure can be clearly visualized, i.e., it still remains in its original crystalline structure. While for the solid solution with solute Cu equal to or greater than 20 at. %, the projection of atomic position is obviously disordered, indicating that the crystal lattice has collapsed and turned into a disordered state, i.e., a crystal-to-amorphous transition has clearly taken place. Figure 4 shows the corresponding density profiles $\rho_\alpha(z)$ for the solid solutions with the alloy compositions of $Cu_5Ru_{95}$, $Cu_{20}Ru_{80}$, and $Cu_{50}Ru_{50}$, respectively. It can be seen that when the solute concentration is less than 20 at. %Cu, the atomic planes can clearly be distinguished from the density profiles; however, once the Cu concentration equals or exceeds 20 at. %, a relatively uniform distributed density profile appears. In order to have firm evidence, the total and partial pair-correlation functions $g(r)$ for hcp Ru-based solid solutions are calculated and shown in Fig. 5. In the figure, as the $g(r)$ curve of $Cu_5Ru_{95}$ shows apparent sharp peaks even at a large distance $r$, the $Cu_5Ru_{95}$ simulation model is considered to be still in a crystalline structure. In comparison, for the $Cu_{20}Ru_{80}$ simulation models, though the first peaks and the second peaks of the $g(r)$ curves are still clear, there are no discernible peaks beyond the third-nearest neighbors. In a classical works, R. Zallen has pointed that the short-range order of amorphous phase is characterized by the clear first- and second-nearest neighbor peaks in the radial distribution function (RDF) and discernible peaks in the RDF rarely occur beyond third-nearest neighbors.[40] Thus, based on Fig. 4 and Fig. 5, one can conclude that a crystal-to-amorphous transition takes place in the $Cu_{50}Ru_{50}$ and $Cu_{20}Ru_{80}$ simulation models. These results clearly indicate that in the Cu-Ru system, when the Cu concentration equals or exceeds 20 at. %, the hcp Ru-based solid solution becomes unstable and turns into an amorphous state.

From the above results, it can be concluded that the critical solid solubility is 20 at. % Cu for the hcp Ru-based solid solutions. Similarly, for the fcc Cu-based solid solution, the critical solid solubility is determined to be 10 at. % of Ru. Consequently, the two critical solid solubilities are determined to be 20 at. % of Cu for hcp Ru-based solid solution, and 10 at. % of Ru for the fcc Cu-based solid solution, re-

TABLE II. Tight-binding potential parameters of the Cu-Ru system used in the present study. $A$ and $\xi$ are expressed in $10^{-19}$ J/at. %, and $r_0$ and $r_{cutoff}$ are expressed in angstroms.

| | $p$ | $q$ | $A$ | $\xi$ | $r_0$ | $r_{cutoff}$ |
|---|---|---|---|---|---|---|
| Cu-Cu | 5.7662 | 1.2313 | 0.1411 | 1.727 | 2.78 | 5.0 |
| Ru-Ru | 19.1540 | 1.6631 | 0.078 58 | 3.1487 | 2.73 | 4.7 |
| Cu-Ru | 10.8624 | 6.6235 | 1.3863 | 6.4895 | 2.649 | 5.0 |

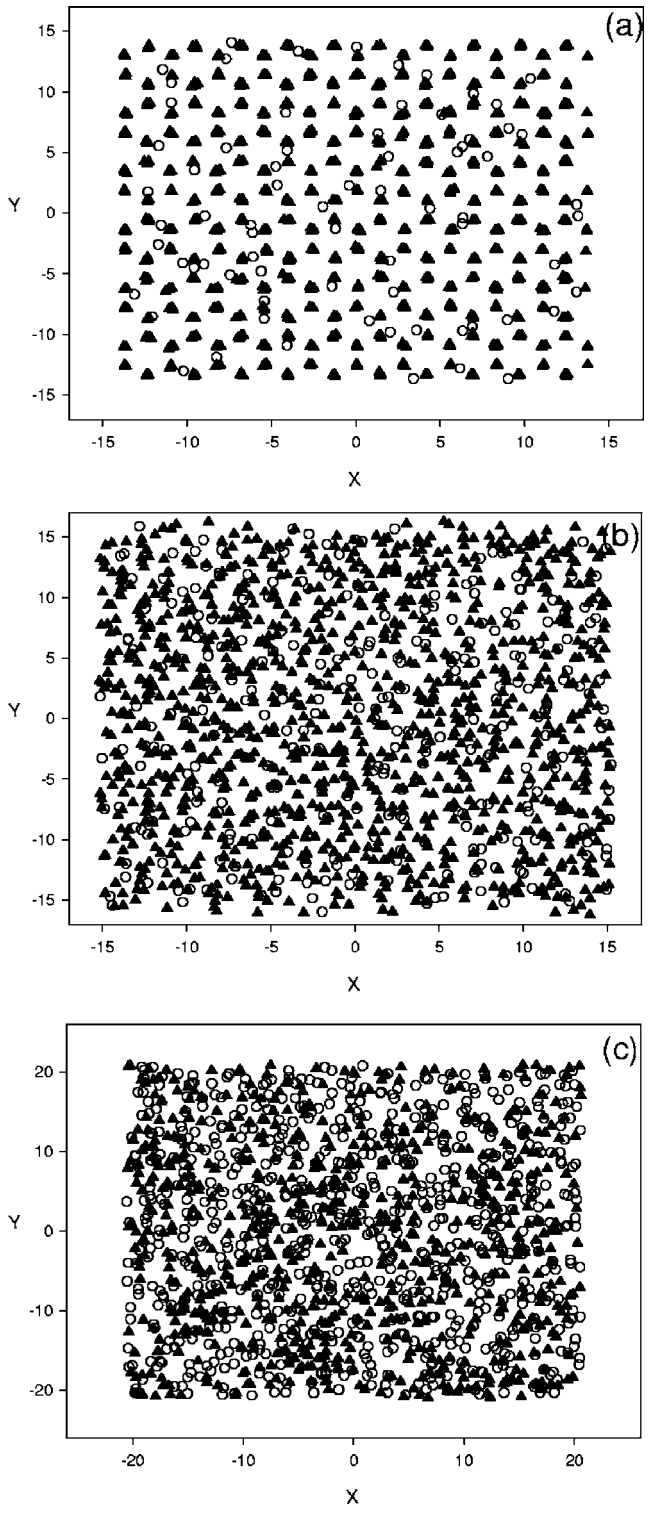


FIG. 3. The projections of atomic positions for the (a) $Cu_5Ru_{95}$, (b) $Cu_{20}Ru_{80}$, and (c) $Cu_{50}Ru_{50}$ hcp solid solutions after annealing at 300 K for 120 000 MD time steps, respectively. Open circles: Cu. Filled triangles: Ru.

spectively. It follows that an amorphous alloy would be formed, when its composition falls into the composition range bounded by the two determined critical solid solubilities and that the GFA/GFR of the Cu-Ru system is therefore within 10–80 at. % of Ru. More interestingly, an amorphous

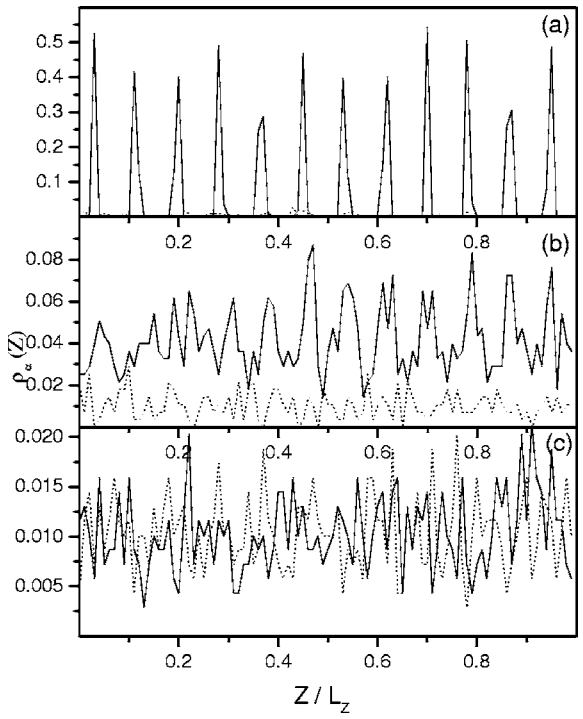


FIG. 4. The calculated density profiles $\rho_\alpha(z)$ of Cu and Ru atoms along the $z$ direction in (a) $Cu_5Ru_{95}$, (b) $Cu_{20}Ru_{80}$, and (c) $Cu_{50}Ru_{50}$ hcp solid solutions after annealing at 300 K for 120 000 MD time steps, respectively. $\rho_{Ru}(z)$ is represented by the solid line and $\rho_{Cu}(z)$ by the dotted line. The ordinate is in arbitrary units.

phase was found at the composition of $Cu_{50}Ru_{50}$ by IBM experiment,[36] which is covered by the theoretically predicted result.

### *2. Interface stability*

We finally present the detailed simulation results observed in the Cu-Ru sandwich model under the temperature of

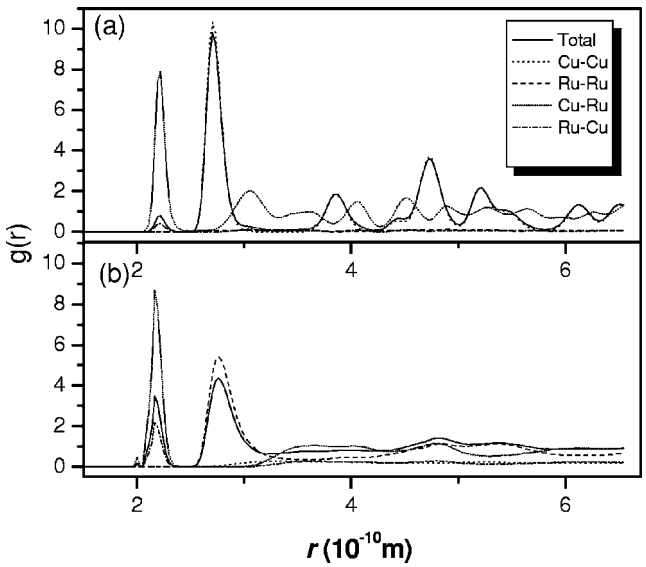


FIG. 5. Total pair-correlation functions $g(r)$ of (a) $Cu_5Ru_{95}$ and (b) $Cu_{20}Ru_{80}$ hcp solid solutions after annealing at 300 K for 120 000 MD time steps, respectively.

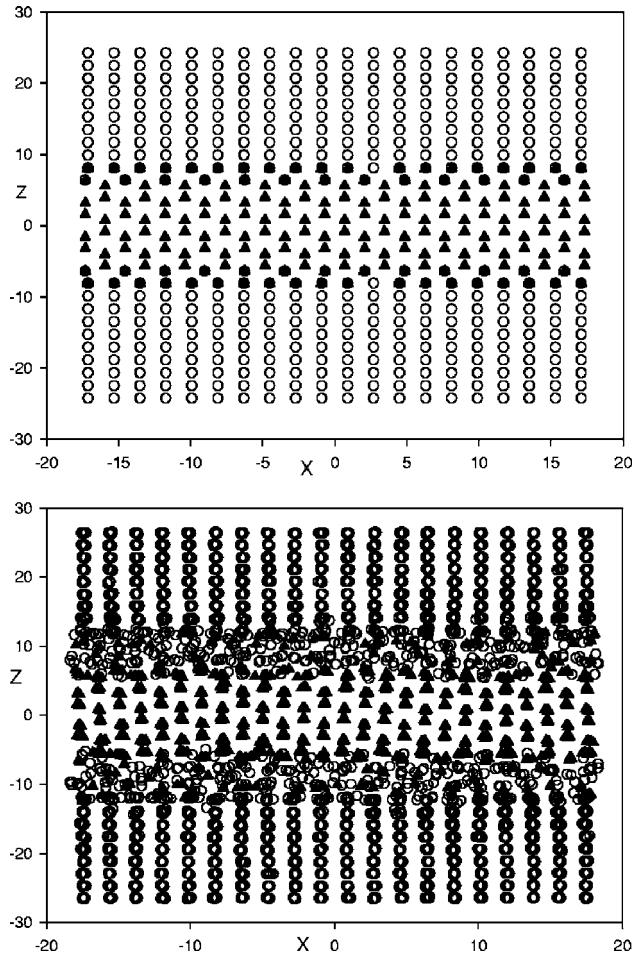


FIG. 6. The schemes of the Cu-Ru multilayers. (a) Configuration of the initial state with preset disordered interlayer between Cu and Ru. (b) The state after solid-state amorphization. The open circle symbols represent Cu and filled triangles represent Ru.

300 K. Figure 6 displays two projections of the atomic positions on the *x*-*z* plane of initial state and after isothermally annealing for 25 ns, respectively. The projections exhibit vividly the process of solid-state amorphization taking place in the Cu-Ru sandwich model. Figure 6(a) is the initial state of the sandwich model, in which some chemical disordering is present at the interface in order to simulate the real situation that in practice, a disordered interlayer could be formed at the Cu/Ru interface. After simulation of 0.05 ns, the majority of the atoms far from the interface in the sandwich model still retain their crystalline structure as in the initial state, whereas those atoms near the interface change into a disordered state, indicating that solid-state amorphization is taking place in the interface. With further increasing the simulation time to 25 ns, Fig. 6(b) shows that the amorphous interlayer does not increase further and remains in a stable thickness.

By carefully inspecting Fig. 6, one can see that the process of the solid-state amorphization features the following two characteristics. First, the growing speed of the amorphous interlayer gradually slows down and eventually approaches zero. Figure 7 shows the change of the Cu and Ru atomic density profiles, $\rho_\alpha(z)$, along the $z$ direction, perpendicular to the interface with increasing MD simulation time steps. Figure 7(a) is the initial state of the sandwich model from which a perfect layered structure can be seen. After MD simulations up to 25 ns, Fig. 7(b) shows that some Ru (Cu) atoms near the interface diffuse into the partner Cu (Ru) lattice and thus result in interfacial amorphization. However, one can note that in the areas far away from the interface, the Cu and Ru lattices still reserve their respective crystalline structures, and the thickness of the amorphization area does not increase with increasing MD simulation time steps. Second, the observed solid-state amorphization in the Cu-Ru system features a so-called asymmetric-growth behavior, as one can see from Figs. 6 and 7 that the disordered interlayer extends faster toward the Cu lattice than toward the Ru direction.[33] As the cohesive energy of Ru is larger that of Cu, therefore one can consider that the Ru lattice is more stable than Cu lattice, i.e., Ru lattice is more difficult to turn into disordered state. It worth noting that the critical solid solubility of Ru in Cu (10 at. %) is smaller than that of Cu in Ru (20 at. %) according to above simulations, which fits well with the result obtained from the sandwich model.

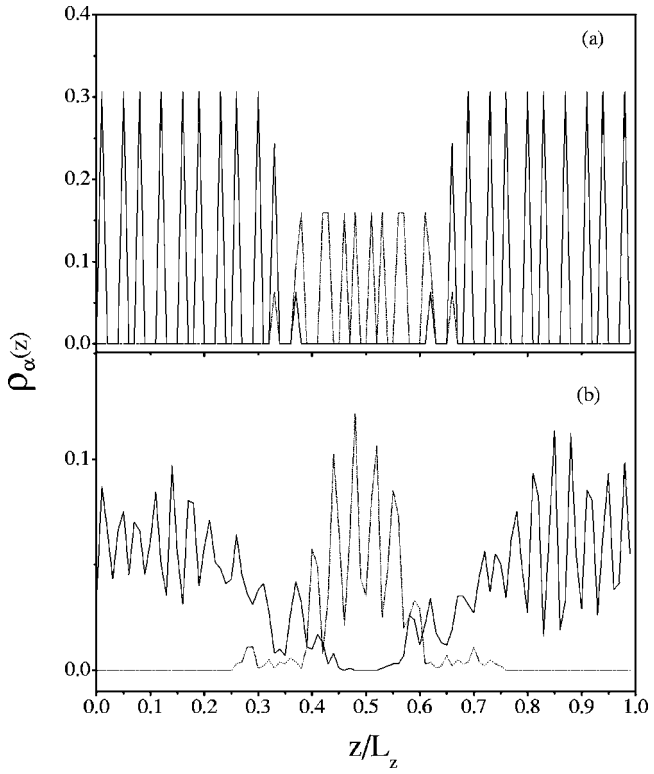


FIG. 7. The density profiles $\rho_\alpha(Z)$ of Cu (solid line) and Ru (dash line) along the $z$ direction at the initial state (a) and the annealing states at 300 K for (b) 25 ns, respectively.

We then make further discussion on the solid-state amorphization in the immiscible Cu-Ru multilayers from the thermodynamic as well as kinetic point of view. According to the model proposed by Lin *et al.*, two necessary conditions have to be satisfied for the solid-state amorphization to take place in a binary metal system.[41] First, the formed amorphous phase should have a lower Gibbs free energy than the initial energetic state of the multilayers, i.e., the thermodynamic factor $\Delta F$, defined as that the energy difference between the

TABLE III. The thermodynamics parameters of Miedema's model and Alonso's method (Ref. 5) used in calculation for the thermodynamic factor $\Delta F$ and the kinetic factor $\kappa$ of the Cu-Ru system.

| | $V$ ($cm^3$) | $\phi^*$ (V) | $n_{ws}$ (density unit) | $\Delta H^{fuse}$ (kJ/mol) | $T$ (K) | $\gamma^0$ ($mJ/m^2$) | $\kappa$ | $\Delta F$ (kJ/mol) | $\Lambda_{max}$ (nm) |
|---|---|---|---|---|---|---|---|---|---|
| Cu | 7.11 | 4.45 | 3.18 | 13.00 | 1358 | 1825 | 1.65 | −17 | 2.91 |
| Ru | 8.20 | 5.40 | 6.13 | 24.29 | 2523 | 3050 | | | |

amorphous phase and the multilayers should be negative. Second, the kinetic factor $\kappa$ should be greater than 0.6 for a transition metal-metal system. According to the definitions, the thermodynamic factor $\Delta F$ and the kinetic factor $\kappa$ can be respectively expressed by

$$\Delta F = \Delta G_{\{AB\}} - 2 \times \left( \gamma_{[A]-\{AB\}} + \gamma_{[B]-\{AB\}} + d_{AB} \frac{\Delta G_{\{AB\}}}{V_{\{AB\}}} \right) \frac{V_{\{AB\}}}{(D_A + D_B)} \tag{7}$$

$$\kappa = 1 - \frac{V_A^{eff}}{V_B} + (T_B - T_A)\left( \frac{1}{T} - \frac{1}{T_B} \right), \tag{8}$$

where $\Delta G_{\{AB\}}$ is the difference of Gibbs free energies between the amorphous state and the crystalline state of the $A$-$B$ alloy (A and B stand for the constituent metals); $\gamma_{\text{A-}\{AB\}}$ and $\gamma_{\text{B-}\{AB\}}$ are the interfacial free energies of the $A$-$\{AB\}$ and $B$-$\{AB\}$ interface, respectively; $D_A$ and $D_B$ are the thicknesses of $A$ and $B$ layers, respectively; $d_{AB}$ is the growing thickness of the amorphous interlayer; $V_{\{AB\}}$ is the mean value of the atom volumes of A and B; $V_A^{eff}$ is effective volume of A in the matrix of the metal B; and $T$, $T_A$, and $T_B$ are the annealing temperature and the melting points of metals A and B, respectively. Concerning the definitions and calculation of those variables, the readers are referred to the published literature.[41] From Eq. (7), by setting $F=0$, one can obtain the following equation to estimate the maximum thickness of the growing amorphous interlayer:

$$\Lambda_{max} = \frac{(\gamma_{[A]-[B]} + \gamma_{[B]-[A]})V_{\{AB\}}}{\Delta G_{\{AB\}}}. \tag{9}$$

Substituting the relevant quantities of the Cu-Ru system into the above equation, one can obtain that the thermodynamic factor $\Delta F$, kinetic factor $\kappa$, and the maximum thickness of amorphous interlays of the Cu-Ru system are −17 kJ/mol, 1.65 and 2.91 nm, respectively. Table III lists the calculated results and the parameters used in the calculation. From Table III, one can clearly see that the thermodynamic factor $\Delta F$ is truly negative and kinetic factor $\kappa$ is greater than 0.6, suggesting that the solid-state amorphization is possible to take place in the Cu-Ru system.

It is important to compare the theoretical calculation results with the experimental result. It has been shown by R. Chan *et al.* that the interfaces can be stable between Cu/Ru(20 nm)/Si after annealing at 720 K, and the Cu/Ru interface has very excellent adhesion ability.[42] Moreover, using Rutherford backscattering and high-resolution analytical electron microscopy, Arunagiri *et al.* showed that 5 nm Ru film can function as a directly plateable Cu diffusion barrier up to at least 573 K vacuum anneal.[43] It is worth noting that the MD simulations are performed at 300 K and under perfect interfacial conditions, while the real interfaces are always complex. The agreement between the MD simulation calculation and experimental results, in this respect, could therefore be considered excellent. The MD simulation calculations indicate that Ru thin film is a promising candidate as a directly plateable Cu diffusion barrier.

### D. Ion beam mixing results

We now present the results of IBM experiment. The real compositions of the as-deposited Cu-Ru multilayered samples as well as the ion-mixed metastable phases in the samples are determined by EDS at various irradiation stages. In order to present the detailed structural transitions emerged in three sets of Cu-Ru multilayered samples and determined the GFR of the Cu-Ru system, we present all the experimental results for the Cu-Ru multilayered samples, which are irradiated to doses ranging from $4\times10^{14}$ $Xe^+/cm^2$ to $5\times10^{15}$ $Xe^+/cm^2$.

In the $Cu_{25}Ru_{75}$ multilayered sample, Fig. 8(a) a is a SAD

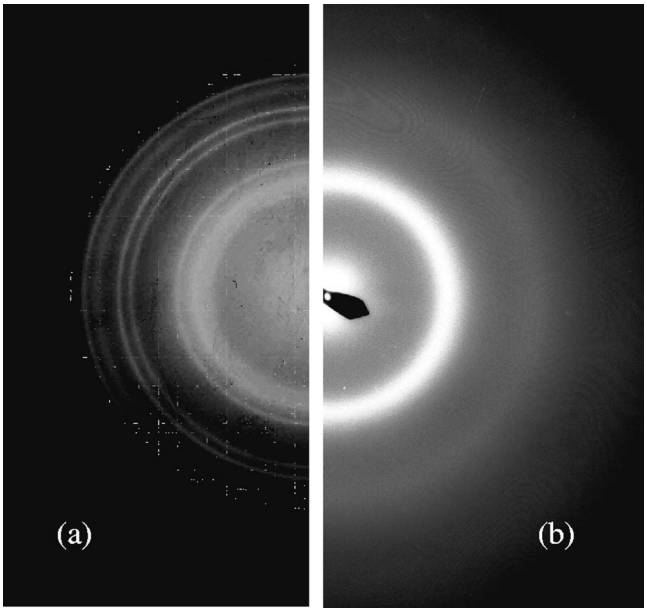


FIG. 8. Selected area diffraction (SAD) patterns for the $Cu_{25}Ru_{75}$ multilayered films of the as-deposited state (a) and amorphous state (b) after irradiation to a dose of $1\times10^{15}$ $Xe^+/cm^2$.

pattern of the as-deposited $Cu_{25}Ru_{75}$ multilayered films. The sharp diffraction lines of polycrystalline Cu and Ru can clearly be observed. After 300 K ion irradiation to a small dose of $2\times10^{14}Xe^{+}/cm^{2}$, the diffraction lines of the polycrystalline Ru became weaker than those in the as-deposited state. With increasing the irradiation dose, the diffraction lines of the polycrystalline Ru showed a tendency to disappear, and at a dose of $1\times10^{15}$ $Xe^{+}/cm^{2}$, an amorphous phase appeared clearly in the sight, as shown in Fig. 8(b). In the $Cu_{50}Ru_{50}$ multilayered sample, an amorphous phase was obtained after irradiation by 200 keV Xe ion at 300 K with a dose of $8\times10^{14}Xe^{+}/cm^{2}$.[36] Similarly, an amorphous phase was also obtained after irradiation by 200 keV Xe ion at 300 K with a dose of $5\times10^{14}Xe^{+}/cm^{2}$.

The IBM results show that amorphous alloys are indeed obtained in the three designed alloy compositions, suggesting that a composition range favoring amorphization is at least from 25 to 75 at. % Ru, which is quite compatible with that predicted by MD simulations, i.e. 10–80 at. % Ru.

Referring again to the MD simulation results, one finds that the above IBM results are in good agreement with the predictions. It is known that IBM is a process far-from-equilibrium and can generally be divided into two steps,[33] i.e., an atomic collision cascade triggered by impinging ions, followed by a relaxation. In the present study, the 200 keV xenon ions triggered the atomic collision cascade, which was responsible for inducing atomic mixing between the Cu and Ru layers in the as-deposited multilayered films. After receiving an adequate ion dose, the Cu and Ru atoms were uniformly mixed and the mixture was most likely in a highly energetic and disordered state. According to the atomic collision theory, the relaxation period is extremely short, which allows only a limited rearrangement of the atoms in the Cu -Ru mixture. Consequently, upon relaxation, the highly energetic and disordered Cu-Ru mixture could reside in one of the possible intermediate states of lower energy, e.g., amorphous state.

## IV. CONCLUDING REMARKS

(1) An *n*-body potential is constructed for the immiscible Cu-Ru system at equilibrium with an aid of *ab initio* calculations for obtaining some physical properties necessary to fit the Cu-Ru cross-potential.

(2) Using the solid solution model, simulations reveal that the Cu-based and the Ru-based solid solutions collapse at their respective critical solid solubilities, i.e., 10 at. % Ru and 20 at. % Cu, thus determining an intrinsic glass-forming range of the system to be within 10–80 at. % Ru, which matches well with the observations in ion beam mixing experiment.

(3) Using the Cu-Ru sandwich model, simulations clarify that the interfacial free energy is the major driving force for interfacial reaction, resulting in spontaneous solid-state amorphization, and that when the interfacial free energy is completely consumed, the reaction terminates, thus determining a maximum amorphous interlayer to be 2.91 nm, which is in good agreement with that predicted by a recently proposed thermodynamic and kinetic model.

(4) Kinetically, simulations further reveal that the growth of the amorphous interlayer features an asymmetric behavior, i.e., the growth advances faster toward the Cu lattice than toward the Ru side, because the critical solid solubility of Ru in Cu (10 at. %) is smaller than that of Cu in Ru (20 at. %).

## ACKNOWLEDGMENTS

The authors are grateful for financial support from the National Natural Science Foundation of China (50531040), the Ministry of Science and Technology of China (2006CB605201), and the Administration of Tsinghua University.

*Author to whom correspondence should be addressed.
Email address: dmslbx@tsinghua.edu.cn

[1] S. P. Murarka, I. V. Verner, and R. J. Gutmann, *Copper-Fundamental Mechanisms for Microelectronic Applications* (Wiley Interscience, New York, 2000).
[2] R. N. Hall and J. H. Racette, J. Appl. Phys. **35**, 379 (1964).
[3] P. K. Wu, G. R. Yang, and T. M. Lu, Appl. Phys. Lett. **65**, 508 (1994).
[4] International Technology Roadmap for Semiconductors, SEMATECH, Inc., Austin, TX (2001).
[5] F. R. de Boer, R. Boom, W. C. M. Mattens, A. R. Miedema, and A. K. Niessen, *Cohesion in Metals: Transition Metal Alloys* (North-Holland, Amsterdam, 1989).
[6] M. W. Lane, C. E. Murray, F. R. McFeely, P. M. Vereechen, and R. Rosenberg, Appl. Phys. Lett. **83**, 2330 (2003).
[7] D. Josell, D. Wheeler, C. Witt, and T. P. Moffat, Electrochem. Solid-State Lett. **6**, C143 (2003).
[8] Q. Wang, J. G. Ekerdt, D. Gay, Y. M. Sun, and J. M. White, Appl. Phys. Lett. **84**, 1380 (2004).
[9] Y. Zhang, L. Long, T. N. Arunagiri, O. Ojeda, S. Flores, O. Chyan, and R. M. Wallance, Electrochem. Solid-State Lett. **7**, C107 (2004).
[10] Z. C. Li, D. P. Yu, and B. X. Liu, Phys. Rev. B **65**, 245403 (2002).
[11] H. Bakker, *Enthalpies in Alloys: Miedema's Semi-Empirical Model* (Trans Tech, Zurich, 1998).
[12] J. M. Lopez and J. A. Alonso, Z. Naturforsch. A **40a**, 1199 (1985).
[13] J. A. Alonso, L. J. Gallego, and J. A. Simozar, Riv. Nuovo Cimento **12**, 587 (1990).
[14] A. R. Miedema and F. J. A. den Broeder, Z. Metallkd. **70**, 14 (1979).
[15] J. Gerkema and A. R. Miedema, Surf. Sci. **124**, 351 (1983).
[16] Z. J. Zhang, O. Jin, and B. X. Liu, Phys. Rev. B **51**, 8076 (1995).
[17] G. Kresse and J. Hafner, Phys. Rev. B **47**, 558 (1993).
[18] G. Kresse and J. Furthmüller, Comput. Mater. Sci. **6**, 15 (1996).

[19] G. Kresse and J. Furthmüller, Phys. Rev. B **54**, 11169 (1996).
[20] J. P. Perdew and A. Zunger, Phys. Rev. B **23**, 5048 (1981).
[21] J. P. Perdew, J. A. Chevary, S. H. Vosko, K. A. Jackson, M. R. Pederson, D. J. Singh, and C. Fiolhais, Phys. Rev. B **46**, 6671 (1992).
[22] J. Monkhorst and J. D. Pack, Phys. Rev. B **13**, 5188 (1976).
[23] H. Vosko, L. Wilk, and M. Nusair, Can. J. Phys. **58**, 1200 (1980).
[24] F. Ducastelle, in *Computer Simulation in Materials Science*, edited by M. Meyer and V. Pontikis, NATO Advanced Study Institute, Series E: Applied Physics (Kluwer, Dordrecht, 1991), Vol. 205.
[25] F. Cleri and V. Rosato, Phys. Rev. B **48**, 22 (1993).
[26] V. Rosato, M. Guillope, and B. Legrand, Philos. Mag. A **59**, 321 (1989).
[27] M. Parrinello and A. Rahman, J. Appl. Phys. **52**, 7182 (1981).
[28] G. Ciccotti and W. G. Hoover, *in Molecular-Dynamics Simulation of Statistical-Mechanical Systems*, ASI-NATO (North-Holland, Amsterdam, 1986).
[29] V. Rosato, G. Ciccotti, and V. Pontikis, Phys. Rev. B **33**, 1860 (1986).
[30] W. B. Pearson, *A Handbook of Lattice Spaces and Structures of Metals and Alloys* (Pergamon, London, 1958).
[31] C. Massobrio, V. Pontikis, and G. Matin, Phys. Rev. B **41**, 10486 (1990).
[32] P. Mura, P. Demontis, G. Suffritti, V. Rosato, and M. Antissari, Phys. Rev. B **50**, 2850 (1994).
[33] B. X. Liu, W. S. Lai, and Z. J. Zhang, Adv. Phys. **50**, 367 (2001).
[34] J. F. Ziegler and J. P. Biersack, *TRIM* (Pergamon Press, New York, 1992).
[35] Z. J. Zhang, O. Jin, and B. X. Liu, Phys. Rev. B **51**, 8076 (1995).
[36] X. He, X. Y. Li, and B. X. Liu, J. Phys. Soc. Jpn. **72**, 3032 (2003).
[37] W. B. Pearson, *A Handbook of Lattice Spaces and Structures of Metals and Alloys* (Pergamon, London, 1958).
[38] E. A. Brandes and G. B. Brook, *Smithells Metals Reference Book*, 7th ed. (Butterworth-Heinemann, Oxford, 1992).
[39] D. R. Lide, *Handbook of Lattice Spaces and Structures of Metals and Alloys* (CRC, New York, 2002).
[40] Richard Zallen, *The Physics of Amorphous Solids* (John Wiley & Sons, New York, 1983).
[41] C. Lin, G. W. Yang, and B. X. Liu, Phys. Rev. B **61**, 15649 (2000).
[42] R. Chan, T. N. Arunagiri, Y. Zhang, O. Chyan, R. M. Wallace, M. J. Kim, and T. Q. Hurd, Electrochem. Solid-State Lett. **7**, G154 (2004).
[43] T. N. Arunagiri, Y. Zhang, and O. Chyan, Appl. Phys. Lett. **86**, 083104 (2005).